Separation and Purification Technology 393 (2026) 137269

Contents lists available at ScienceDirect

Separation and Purification Technology

journal homepage: www.elsevier.com/locate/seppur

Small scale hydraulic membrane resistance measurement by analytical multi-sample photo-centrifugal filtration (ACF)☆

Philipp Lösch [a], André Lier [a], Nikolai Benz [a], Sebastian Boldt [b], Dietmar Lerche [b], Sergiy Antonyuk [a,*]

[a] Institute of Particle Process Engineering, RPTU University Kaiserslautern-Landau, 67663 Kaiserslautern, Germany
[b] LUM GmbH, 12489 Berlin, Germany

ARTICLE INFO

Editor: B. Van der Bruggen

Keywords:
Membranes
Characterization
Analytical photo-centrifugal filtration
Filtration theory

ABSTRACT

The continuous development of new products in pharmaceutical and biotechnology industries requires efficient and scalable separation processes. Standardized laboratory tests for hydraulic resistance of filtration membrane typically demand large membrane areas and substantial suspension volumes. Analytical photo-centrifugal filtration (ACF) offers a novel approach for high-throughput membrane characterization using minimal sample volumes. Based on continuous in-situ measurement of space- and time-resolved light transmission, ACF determines filtrate volume via STEP-Technology®. Unlike conventional pressure-driven methods, ACF operates without external pressure and requires minimal cleaning. Its flexible design allows parameter adjustments by varying rotor speeds or temperature profiles within a single experiment. In contrast to the conventional method (VDI 2762), several samples can be measured at once. This study presents an improved filtration cell for ACF and demonstrates the comparability of membrane resistances measured by ACF and VDI 2762. A polypropylene membrane with a nominal pore size of approximately 0.1 µm was used. Challenges and future opportunities are also discussed.

1. Introduction

The separation of particles from dispersions is an important unit operation across various industries, serving both the production and refinement of valuable particulate materials, as well as the purification of liquids. Among the different separation methods, filtration stands alongside sedimentation as one of the most essential processes for separating solids from liquids. While the effect of solids retention can differ between surface, depth and crossflow filtration, it is essential to identify a suitable filter medium tailored to the specific separation mechanisms [1]. The development or selection of an optimal filter medium is typically a complex and time-intensive process, involving extensive filtration tests conducted at laboratory and/or pilot-plant scale. For these tests, standardized filter housings in the form of a pressure or vacuum filtration are often used [2–5]. An essential parameter to be determined is the filter medium resistance, which can be dependent on pressure and on the used solvent.

A widely used method for measuring the filter medium resistance is described in the guideline VDI 2762 [2] and further referenced in [6–8]. This method has been applied in several recent studies [9–14] and is commonly used in industry. With advancements in bio- and nanotechnology, new challenges arise, particularly due to the limited availability and high cost of sample materials. Furthermore, selecting an appropriate filter medium requires careful consideration of not only the high separation efficiency requirements but also of the interactions between the filter medium and the liquid components. These interactions influence the particle adhesion and the constituent adsorption on the filter medium, affecting its permeability and cleaning requirements. Consequently, the continuous development of novel membranes and surface modifications remains essential [15].

The diversity of available filtration materials introduces additional complexity, beginning with the distinction between organic and inorganic membrane raw materials [16]. Especially when using membranes for the filtration of dispersions (suspensions, emulsions as well as colloidal solutions), extensive test series with several different filter media are typically required [17]. Filtration experiments for determining filter resistances using standardized filter housings [2] require

☆ This article is part of a Special issue entitled: 'WFC14' published in Separation and Purification Technology.

* Corresponding author.
E-mail address: sergiy.antonyuk@mv.rptu.de (S. Antonyuk).

https://doi.org/10.1016/j.seppur.2026.137269
Received 14 October 2025; Received in revised form 26 January 2026; Accepted 11 February 2026
Available online 13 February 2026

Nomenclature

List of symbols

A	Filtration area, m^2
h_{FC}	Filter cake height, m
k	Ratio of filter cake volume to filtrate volume, –
n	Rotational speed, rpm
p	Pressure, Pa
Δp_{FC}	Pressure drop across the filter cake, Pa
Δp_{FM}	Pressure drop across the filter medium, Pa
Δp_{tot}	Total pressure drop, Pa
r	Radial distance, m
r_l	Radial distance of the liquid column to the center of rotation, m
r_m	Radial distance to the filter medium, m
R_{FC}	Filter cake resistance, m^{-1}
R_{FM}	Filter medium resistance, m^{-1}
t	Time, s
v_F	Specific filtrate flux, $l \bullet m^{-2} \bullet h^{-1} \bullet bar^{-1}$
V	Volume, m^3
V_{FC}	Filtrate volume with respect to the filter cake resistance, m^3
V_{FM}	Filtrate volume with respect to the filter medium resistance, m^3
V_{tot}	Total filtrate volume, m^3

Greek letters

α_H	Specific cake resistance, m^{-2}
ρ_l	Fluid density, $kg \bullet m^{-3}$
η	Dynamic viscosity, Pa•s
ω	Angular velocity, $rad \bullet s^{-1}$

large volumes of test suspension (100–300 ml per test) and significant areas of filter media (55 mm to 60 mm in diameter). The use of such sample quantities in biotechnology or nanotechnology is not only associated with substantial costs but also poses high ecological risks, particularly when hazardous substances are involved. The use of smaller filter media samples offers distinct advantages, allowing for a high number of filtration performance tests during the development phase. In particular, membranes may exhibit spatial inhomogeneities, leading to variation in hydraulic resistance across the membrane surface. Such effects can be systematically investigated using the proposed experimental approach by performing repeated measurements on different regions of the membrane sample. Moreover, small-scale filtration measurements are particularly valuable for validating detailed and computationally intensive filtration simulations [9,18–21].

This study investigates and further refines analytical photocentrifugal filtration (ACF) [22], a multi-sample method that requires only minimal suspension volumes and small membrane sizes. ACF facilitates rapid estimation and optimization of effective suspension/emulsion and filter medium combinations compared to conventional methods [23]. Previous investigations showed ACF's capability in determining filter medium resistance [24], analyzing the consolidation of compressible filter cakes [24,25] and assessing membrane fouling effects [26]. Until now, ACF tests could not be performed under constant pressure, as summarized by Loginov et al. [23]. The presented work aims to establish operating conditions that enable direct comparison between ACF experiments and standardized tests according to VDI 2762. This includes defining a function for rotor speed and implementing a multi-stage experimental protocol, following the methodology of Loginov et al. [24].

2. Materials and methods

2.1. Methods

2.1.1. Standard filtration test

Fig. 1 shows the schematic setup of the filtration test setup according to VDI 2762 [2]. For comparative measurements, a conventional filtration cell is employed, with a fluid volume of approximately 250 ml and a filter area of 20 cm^2. The filtrate flow rate is obtained by measuring the mass over time. A prerequisite for accurate measurement is the maintenance of constant pressure throughout the filtration time. A constant fluid pressure is maintained using compressed air. After setting the desired differential pressure with a proportional pressure regulator (VPPE, FESTO SE & Co. KG), the cell is closed, and the pressure is applied. In order to prevent oscillations of the balance caused by a pressure surge when opening the air pressure valve, a hydraulically coupled outlet was implemented [27]. As shown in Fig. 1, the drainpipe, which extends below the liquid level in the filtrate collection tank, is equipped with a shut-off valve that allows the drainpipe to be filled (vented) before the experiment begins [13]. The filtrate mass recording is initiated, followed by opening the shut-off valve. At the end of the experiment, when no further changes in filtrate mass are observed, the pressure is released, and the housing is opened.

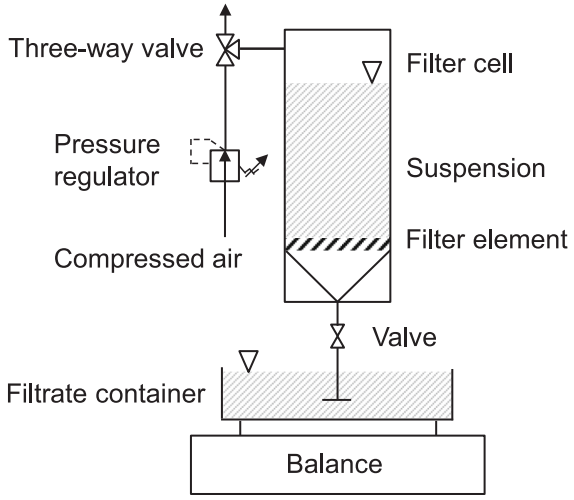

Fig. 1. Standard experimental setup according to VDI 2762 [10].

The flow through porous media is described by the Darcy equation Eq. (1). It expresses the volume flow rate through the filter medium (FM) as the ratio of the total pressure difference Δp across the filtration area A to the total filter medium resistance R_{FM}, normalized by the viscosity η of the continuous phase [28].

$$\frac{dV_{FM}}{dt} = \frac{\Delta p_{FM} \bullet A}{\eta \bullet R_{FM}} \tag{1}$$

The volume flow rate through the formed cake depends on the time-dependent cake resistance R_{FC} as

$$\frac{dV_{FC}}{dt} = \frac{\Delta p_{FC} \bullet A}{\eta \bullet R_{FC}(t)} \tag{2}$$

Assuming an incompressible filter cake, the cake resistance is only dependent on the volume specific resistance of the cake α_H and its height h_{FC} at time t:

$$R_{FC}(t) = h_{FC}(t) \bullet \alpha_H \tag{3}$$

At a constant solid concentration and in the absence of creaming or sedimentation, the height-to-volume ratio of the filter cake remains constant:

$$h_{FC}(t) = \frac{k}{A} \bullet V(t) \tag{4}$$

Where k is the ratio of the cake volume to the filtrate volume. Incorporating the pressure drops, the total filtrate volume flow through both the filter medium and filter cake can be determined as:

$$\frac{dV_{tot}}{dt} = \frac{\Delta p_{tot} \bullet A}{\eta \bullet (R_{FM} + R_{FC}(t))} \tag{5}$$

At a constant pressure drop, Eq. (5) can be integrated into:

$$t = \frac{k \bullet \eta \bullet \alpha_H}{2 \bullet A^2 \bullet \Delta p_{tot}} \bullet V^2(t) + \frac{R_{FM} \bullet \eta}{A \bullet \Delta p_{tot}} \bullet V(t) \tag{6}$$

This can be rearranged into a linear equation to determine both the specific cake resistance (α_H) and filter medium resistance (R_{FM}).

$$\frac{t}{V} = \frac{k \bullet \eta \bullet \alpha_H}{2 \bullet A^2 \bullet \Delta p_{tot}} \bullet V + \frac{R_{FM} \bullet \eta}{A \bullet \Delta p_{tot}} \tag{7}$$

In the experiments carried out here, only the pure membrane resistance was determined using deionized water. Therefore, the first term of Eq. (7) can be neglected. The calculated filter medium resistance R_{FM} is determined from the y-intercept of the t/V-V diagram, which is derived from the measurement data.

$$\frac{t}{V} = \frac{R_{FM} \bullet \eta}{A \bullet \Delta p_{tot}} \tag{8}$$

2.1.2. Analytical photo-centrifugal filtration (ACF)

The core instrument for ACF is the analytical photo-centrifuge (LUMiSIZER® 615–124, LUM GmbH, Berlin, Germany), which is used for dispersion characterization [29]. The photo-centrifuge features a multi-sample rotor capable of holding up to 12 samples in filtration reservoirs within the filtration cells, which are positioned radially. The rotor speed is adjustable up to 4000 rpm, and temperature control can be set between 4 and 60 °C. This device utilizes linearly parallelized monochromatic light that passes through the transparent polycarbonate walls of the filtration reservoir (Fig. 2).

The transmitted rays are detected and recorded over the entire height of the filtrate reservoir with a spatial resolution of about 14 µm and a finest time resolution of 1 s. The recorded data represent the extinction as a function of the location and time. In Fig. 2 is shown: a) is the transmission profile at the beginning of the centrifugation with a small amount of filtrate (red line), b) the transmission profile at later stages (light and dark green lines), (1) the light source, (2) the parallel light beam, (3) the filtration cell, (4) the multi-sample rotor and (5) the line detector.

Using the optical sensor system of the analytical centrifuge, the filtrate height can be determined in situ automatically, spatially, and temporally resolved. This measurement is based on the analysis of the meniscus formed at the air-filtrate interface, whose geometry depends essentially on the surface tension of the filtrate in contact with the filtration cell wall material. The meniscus shows a strong local drop in the transmission profile. Depending on the filling level, this minimum changes its position as the filtration time progresses. The filtrate volume is obtained from a calibration function that relates the radial position of the meniscus to the corresponding filtrate volume (see Fig. 8 in Section 2.2). Due to the increasing filtrate volume, the meniscus position may shift as the centrifugal acceleration acting on the meniscus decreases. This effect is accounted for by the calibration function. The specially developed filtration cell for ACF is shown in Fig. 3. These cells are constructed from stainless steel (VA) or polyetheretherketone (PEEK) and feature a two-part design comprising a cartridge and a filter medium holder. The filter medium is positioned in the socket. A flat filter medium sample with a diameter of 7 mm can be used. The filtration area of 7.854 mm^2 corresponds to the pore size of the support structure. The two-part assembly is then screwed together and sealed by means of a sealing ring. This filtration module is fixed in a modified disposable standard cuvette and sealed with a stopper. The module allows sample volumes of up to 1 ml, facilitating precise filtration studies.

In centrifugal-field filtration, the pressure is governed by the fluid height above the filter medium and the centrifugal acceleration. Fig. 4 shows the schematic structure of the filtration module in the centrifugal field.

The determination of the filter medium resistance is achieved by measuring the flow of a pure liquid through the filter medium. The liquid should ideally be the continuous phase of the suspension. The pressure above the filter medium results from the radial distance of the liquid column to the center of rotation r_l, the angular velocity ω, the density of the fluid ρ_l, and the radial distance to the filter medium r_m:

$$p(r_m) = \int_{r_l}^{r_m} \rho_l \omega^2 r \, dr = \frac{\rho_l \omega^2}{2} \left({r_m}^2 - {r_l}^2 \right) \tag{9}$$

Since very thin filter media are used, their thickness can be

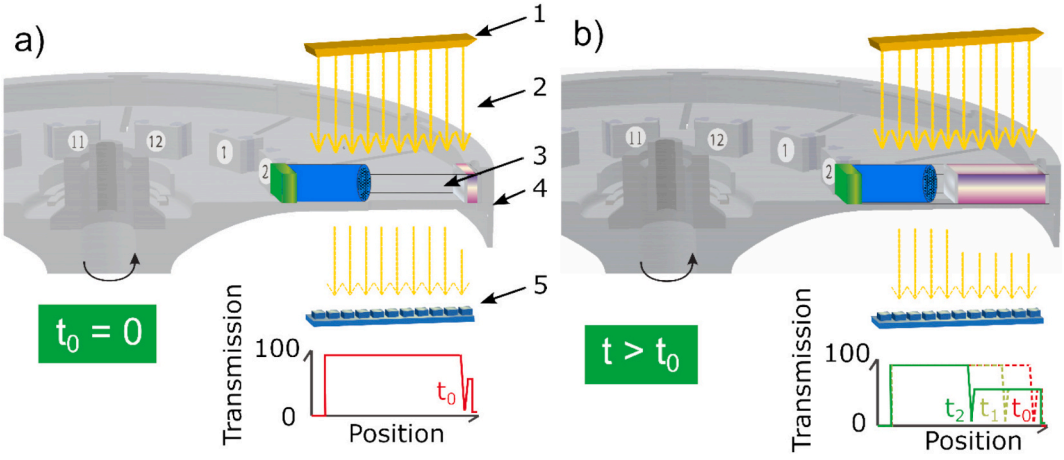

Fig. 2. Schematic representation of the time- and space-resolved extinction profiles in the analytical photo-centrifuge, a) is the transmission profile at the beginning of the centrifugation with small amount of filtrate volume (red line), b) the transmission profile at later stages (light and dark green lines), (1) the light source, (2) the parallel light beam, (3) the filtration cell, (4) the multi-sample rotor and (5) the line detector. (For interpretation of the references to colour in this figure legend, the reader is referred to the web version of this article.)

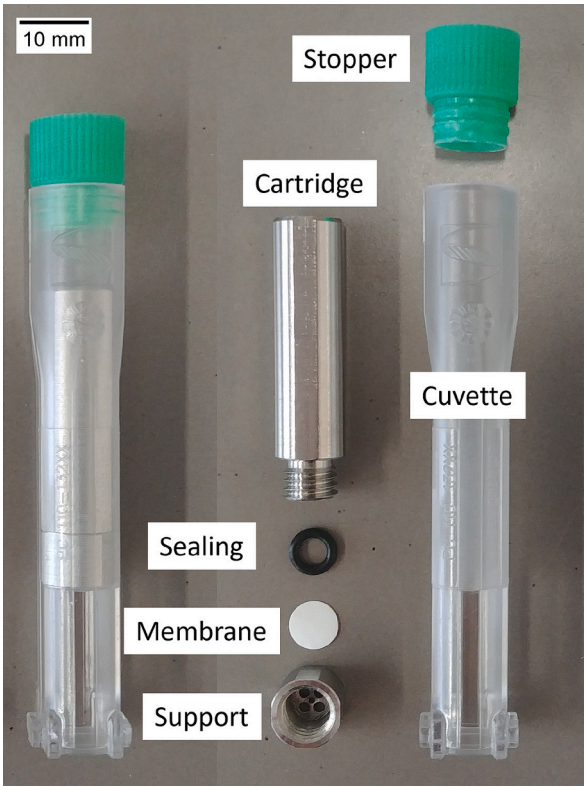

Fig. 3. Cuvettes for the ACF. Left: Assembled cuvette with the filtration cartridge inside. Center: Filter media holder, filter medium, sealing and cartridge which contains the suspension during the experiment. Right: Modified cuvette, which enables the insert of the filter cell.

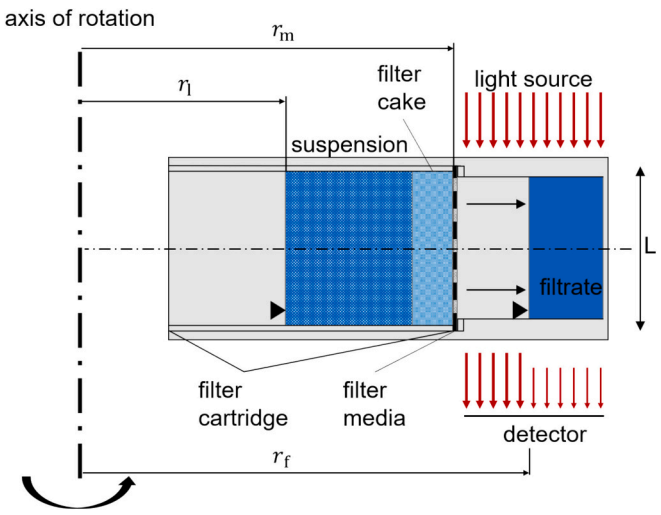

Fig. 4. Schematic of the filter cuvette in a centrifugal field.

considered negligible. With increasing filtration time from the initial state, the distance from the center of rotation to the surface of the liquid column r_l above the membrane increases and the actual height (r_m - r_l) decreases. The pressure thus decreases continuously at constant rotor speed. Eq. (9) applies only when pure fluids are used as was done in this work.

2.2. Materials

For the filtration experiments conducted in accordance with VDI 2762 [2], a pressure housing filtration device TMG 400 (BHS-Sonthofen GmbH) was used. Microporous polymer flat membranes made of polypropylene (Accurel PP^{TM} 1E, 3 M) with a transmembrane flow rate of 2.9 ml/(min*cm^2*bar), a mean pore size of 0.1 µm, a bubble Point of 1.98 bar and a thickness of 102 µm served as the filter media in this study. An SEM image of the membrane surface is shown in Fig. 5.

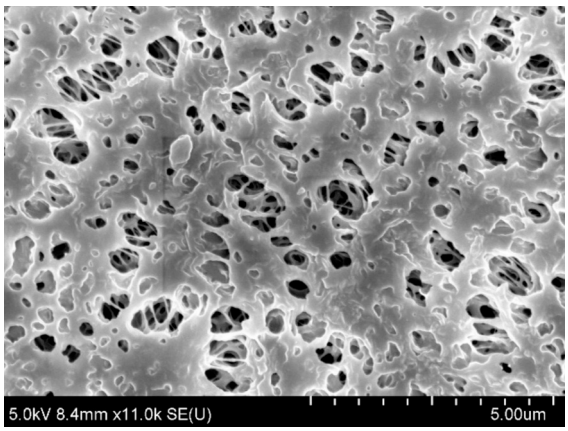

Fig. 5. SEM image of the Accurel PP 1E membrane surface.

Due to their hydrophobicity, the filter media is pre-wetted with ethanol before the experiments. Since the used membranes are very thin (about 100 µm), additional support is required when using conventional pressure housing. A steel fabric made of stainless steel (VA) with a mesh size of 250 µm is used for this purpose. Fully demineralized water is used as a continuous phase.

3. Results

3.1. Implementation of constant filtration pressure during centrifugation

To achieve comparability with the conventional filtration cell according to VDI 2762 and to apply Eq. (6), which assumes a constant filtration pressure, the ACF must be controlled with an increasing rotational speed to maintain a constant pressure. The required speed function can be calculated using Eq. (9), based on the actual filtrate flow. To estimate the filtration time and to program the software, a filter medium resistance of $7.5 \bullet 10^{10}$ m^{-1} was used, based on the previously determined values of the filter medium resistances. Fig. 6 presents the theoretically necessary rotational speed for a constant pressure (red line), calculated using a radial distance of the membrane of $r_m = 107$ mm, the programmed speed function (blue line) and the measured rotational speed during the experiments (black line).

Fig. 6 shows the speed function, assuming an invariant filter medium resistance that ensures constant filtration pressure and, consequently, a stable filtrate flow. For the control of the centrifuge, a speed ramp was developed, which deviates from the required pressure by a maximum of 5 %. With this speed ramp, filtration under constant pressure is provided. To evaluate the effectiveness of this speed ramp in maintaining a constant filtration pressure drop, comparative tests were carried out under both constant pressure and constant rotational speed. The filter medium resistance was determined using a pretreated membrane (wetted with ethanol) and purified water (1 ml). Fig. 7 shows light transmission curves obtained in these experiments using a constant rotational speed (left) and a continuously adjusting speed to maintain constant pressure (right).

The transmission profile evolves from red (initial profile, start of centrifugation) to green (final profile, end of filtration), with uniform time intervals of 60 s between profiles. The minimum of the transmission profile identifies the phase boundary of the liquid filtrate and the air inside the cuvette. When operating at a constant rotational speed, the intervals

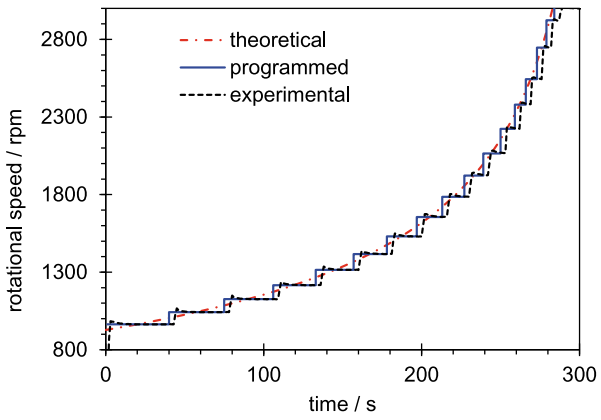

Fig. 6. Increasing speed ramp for filtration at constant pressure.

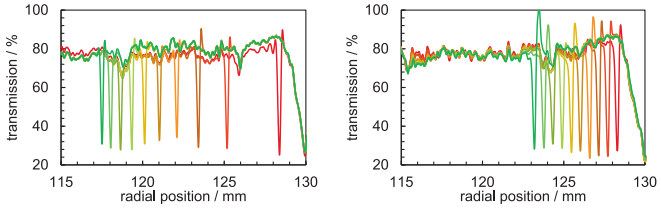

Fig. 7. Transmission profiles of the ACF (profile development over time from red to green) left: constant rotor speed, right: constant pressure using a rotor speed ramp. (For interpretation of the references to colour in this figure legend, the reader is referred to the web version of this article.)

between local transmission minima of each profile in Fig. 7 (left) decrease with increasing filtration time, indicating a decline in both flux and pressure. The longer the filtration, the smaller the increase of the filtrate volume. In contrast, filtration performed at constant pressure using the developed speed ramp maintains nearly identical distances between transmission minima, suggesting a stable filtrate flow over time (Fig. 7 (right)). Additionally, the absolute value of the transmission minimum remains similar over time, and the maximum filtration volume is reached in nearly half the time compared to the filtration test at constant rotational speed. Based on the measurements performed with demineralized water, a calibration function (Fig. 8) was established that describes the relationship between the absolute radial position of the meniscus and the corresponding filtrate volume. The measurements with varied water volumes showed that centrifugal acceleration had only a negligible effect on the meniscus shape and consequently on the calibration curve, and was therefore disregarded, with an average deviation in radial position of only

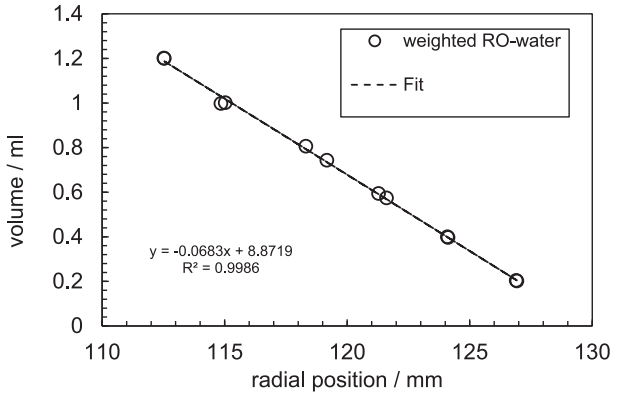

Fig. 8. Function for determining the filtrate volume inside the cuvette from the position of the meniscus.

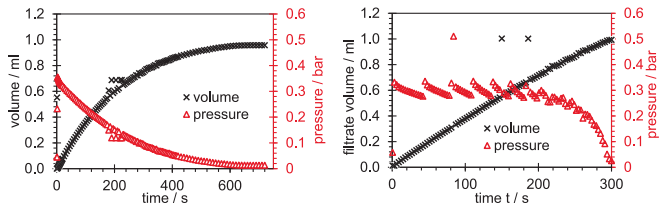

Fig. 9. Filtrate volume (black) and pressure (red) over time of filter media tests conducted with ACF. Left: filtration under constant rotor speed, right: filtration at constant pressure using the computed speed ramp function. (For interpretation of the references to colour in this figure legend, the reader is referred to the web version of this article.)

±0.05 mm. The measuring points were obtained with a varied mass (accuracy ±1 mg) at a controlled temperature inside the centrifuge. A LUMiSIZER® cuvette (10 mm, polycarbonate) was used for the filtrate collection. Since the viscosity and the contact angle of the fluid influence the shape of the meniscus, individual calibration is required for each liquid. In Fig. 8, the circles symbolize actual data points from experiments, while the straight line denotes the calculated fit model, clearly illustrating a linear dependence between volume and radial position.

Using the obtained calibration function, the filtrate volume was determined from the transmission profiles shown in Fig. 7. Fig. 9 shows the filtrate volume and the calculated pressure over time.

Fig. 9 (left) illustrates the results of filtration at a constant rotor speed, where the pressure starts at 0.35 bar (red marks) and gradually decreases over filtration time. Therefore, the slope of the filtrate volume over time (flux) also declines (black marks). By 600 s, the filtration of 1 ml is nearly complete. On the right side of Fig. 9, the detected filtrate volume and calculated pressure are shown for the experiment using the obtained rotor speed ramp function. In this case, the filtration is completed in approximately 300 s. Due to the increasing centrifugal force, the pressure remains nearly constant at 0.3 bar over a 200 s period, resulting in a sawtooth profile. The slope of the filtrate volume is nearly linear, which is expected for a constant pressure filtration of a filter medium without particles in the fluid. The filter media resistance was determined using Eq. (8) following the conventional evaluation method.

3.2. Filter media resistance

The results of filtration experiments conducted with the VDI filtration cell at different pressures, as well as with ACF at constant and increasing rotor speed are shown in Fig. 10. At least three individual measurements were performed and analyzed for each membrane sample. The error bars indicate the variability of the measurement data, specifically the mean value with the standard deviation.

In Fig. 10 (left), after a short initial period, a constant value is reached indicating stable flow resistance over time. Consequently, the filter media resistance can be determined. In Fig. 10 (right), the results of experiments performed with ACF are shown. The filtration experiments were conducted at two different pressures and at a constant rotor speed. Based on the detected filtrate flow and the calculated pressure, the resistance of the filter media can be calculated. By definition, the filter media resistance is a material property that remains independent of pressure, provided that no deformation of the filter material occurs.

Fig. 11 shows the results of measurements performed using both the VDI filtration cell and ACF. In tests conducted at constant rotor speed, the pressure at the start of the filtration was recorded and it was assumed that the starting volume changes only minimally as the required speed was reached very quickly. At low pressure (rotational speed n = const.), the filter media resistance measured with ACF tests is slightly lower than that obtained with the filtration cell. At higher pressures, ACF tends to overestimate resistance, primarily because the actual pressure is not

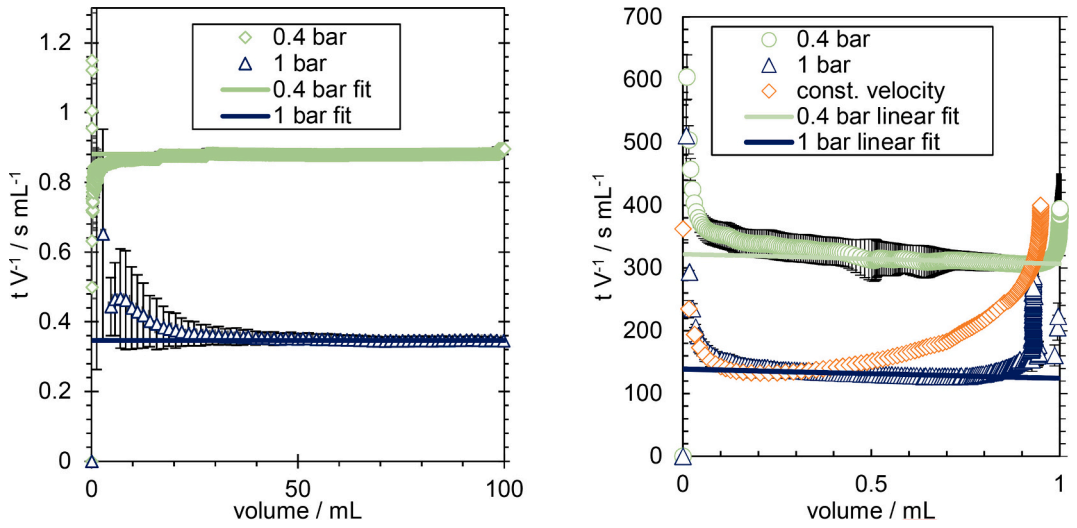

Fig. 10. Plots of t/V versus V for filtration with pure liquid, obtained using the VDI filtration cell (left) and the ACF test (right).

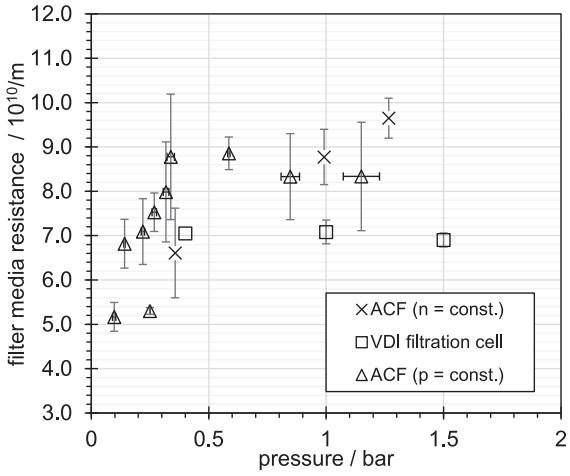

Fig. 11. Filter medium resistance over filtration pressure, measured using the conventional filtration cell and the ACF setup.

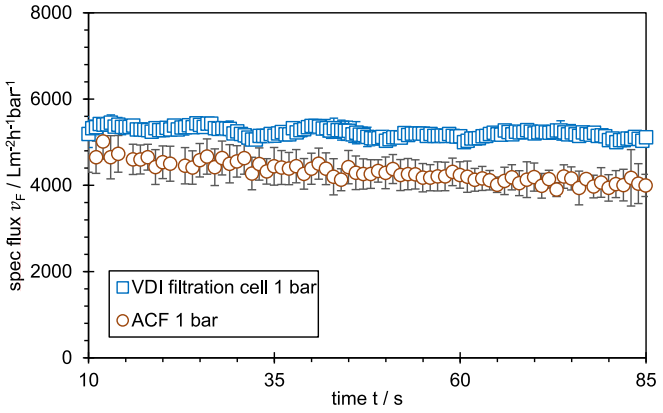

Fig. 12. Specific filtrate flux over time obtained using the VDI filtration test and ACF test.

directly measurable. However, the results obtained with ACF at constant pressure are closer to the experimental values obtained using the VDI 2762 filtration cell. For pressure levels between 0.1 bar and 0.5 bar, ACF experiments under constant pressure indicate a slightly higher resistance of the filter medium compared to VDI 2762. However, as pressure increases, the associated pressure error in constant-pressure ACF experiments also rises. This is attributed to shorter intervals of increasing rotor speed at higher pressure levels, which directly influence filtration flux.

It has been demonstrated that, due to the permitted speed limitation and the specific design conditions of the ACF, a maximum filtration pressure of about 1.2 bar can be achieved under constant pressure conditions.

An alternative approach for directly comparing experiments conducted with both devices and with the standard filter cell is to determine the specific volume flow of the filtrate v_F, which is related to the actual filtration area and effective pressure. Fig. 12 shows the specific filtrate flow over time for a particle-free filtration process. The results indicate that constant-pressure experiments conducted with the ACF exhibit strong agreement with those obtained using the standard filter cell.

4. Conclusion

The study presents a fast and accurate method for determining filter resistances requiring only small suspension volumes. Analytical photocentrifugal filtration (ACF) enables the rapid processing of multiple small filtration batches, significantly reducing the effort compared to conventional VDI 2762 measurements. The filtration results obtained with ACF filter cells show strong agreement with those from standard filter cell experiments.

To ensure constant filtration pressure during ACF tests, a speed ramp was developed and successfully applied. By gradually increasing the rotor speed, reliable resistance measurements under constant pressure conditions were achieved, closely matching the results from conventional methods.

ACF has proven to be a smart, fast, ecological, and cost-efficient approach for characterizing and optimizing membrane filter media. This is particularly beneficial for applications involving valuable or hazardous materials, where efficient material use and process optimization are critical. The developed speed ramp also allows flexible adjustment of operating parameters, supporting adaptive testing strategies in future studies.

Further investigations will focus on enhancing the visibility of the suspension meniscus and characterizing filter cake growth during filtration. This will enable the determination of filter cake resistance and the analysis of cake consolidation or sediment height reduction during

centrifugation - key aspects for evaluating compressible filter cakes. Achieving this will require a redesigned cuvette system, as previously proposed by Radel et al. [30].

CRediT authorship contribution statement

Philipp Lösch: Writing – original draft, Visualization, Validation, Methodology, Investigation, Formal analysis, Data curation, Conceptualization. **André Lier:** Writing – review & editing, Writing – original draft, Visualization, Validation, Investigation, Formal analysis, Data curation. **Nikolai Benz:** Writing – review & editing, Writing – original draft, Visualization, Validation, Investigation, Formal analysis, Data curation. **Sebastian Boldt:** Methodology, Conceptualization. **Dietmar Lerche:** Supervision, Resources, Project administration, Funding acquisition. **Sergiy Antonyuk:** Supervision, Resources, Project administration, Funding acquisition.

Funding

The “Smart batch processes in the energy system of the future” project was made possible by funding from the Carl-Zeiss-Stiftung.

Declaration of competing interest

The authors declare no conflicts of interest. The funders had no role in the design of the study; in the collection, analyses, or interpretation of data; in the writing of the manuscript; or in the decision to publish the results.

References

[1] S. Ripperger, W. Gösele, C. Alt, T. Loewe, Filtration, 1. Fundamentals. *Ullmann's Encyclopedia of Industrial Chemistry*, Wiley-VCH Verlag GmbH & Co. KGaA, Weinheim, Germany, 2000, pp. 1–38. ISBN 9783527306732.
[2] Verein Deutscher Ingenieure, *Filtrierbarkeit von Suspensionen: Bestimmung des Filterkuchenwiderstands*, Beuth Verlag GmbH, Berlin, 2010. *71.040.40* (2762 Blatt 2).
[3] Verein Deutscher Ingenieure, *Mechanische Fest-Flüssig-Trennung durch Kuchenfiltration: Übersicht*, Beuth Verlag GmbH, Berlin, 2006. *71.04.40* (2762 Blatt 1).
[4] H. Anlauf, H. Anlauf, Wet Cake Filtration: Fundamentals, Equipment, Strategies, WILEY VCH, Weinheim, 2020. ISBN 978–3–527-34606-6.
[5] H. Schubert (Ed.), Handbuch der Mechanischen Verfahrenstechnik, John Wiley & Sons, Hoboken, 2003. ISBN 3527305777.
[6] C. Tien, Introduction to Cake Filtration, 1st ed., Elsevier, Amsterdam, 2006.
[7] H. Anlauf, Standardfiltertests zur Bestimmung des Kuchen-und Filtermediumwiderstandes bei der Feststoffabtrennung aus Suspensionen (Teil 2), Filtrieren Separieren 8 (1994) 107–126.
[8] H. Anlauf, Standardfiltertests zur Bestimmung des Kuchen-und Filtermediumwiderstandes bei der Feststoffabtrennung aus Suspensionen (Teil 1), Filtrieren Separieren 8 (1994) 63–70.
[9] V. Puderbach, K. Schmidt, S. Antonyuk, A coupled CFD-DEM model for resolved simulation of filter cake formation during solid-liquid separation, Processes 9 (2021) 826, https://doi.org/10.3390/pr9050826.
[10] F. Sauer, H. Henn, U. Peuker, B. Hoffner, Experimental study on mechanical dewatering and displacement washing of filter cakes with inhomogeneous cake geometry, Sep. Purif. Technol. 349 (2024) 127904, https://doi.org/10.1016/j.seppur.2024.127904.
[11] N. Setargew, G. Harris, U. Kieu, N. Truong, J. Prakasha, Measurement of levels of dross intermetallic particles in 55%Al-Zn alloy based metal coating bath by pressure filtration technique, *Corrosion* Sci. Technol. 23 (2024) 527–537, https://doi.org/10.14773/cst.2024.23.6.527.
[12] E. Löwer, C. Makowlew, T. Leißner, U.A. Peuker, Wetting behavior of porous structures: three-dimensional determination of the contact angle after filter cake dewatering using X-ray microscopy, Adv. Water Resour. 151 (2021) 103894, https://doi.org/10.1016/j.advwatres.2021.103894.
[13] N. Benz, P. Lösch, S. Antonyuk, Influence of the measurement resolution on the filtration analysis: an improved test setup according to VDI 2762 guideline, Processes 11 (2023) 299, https://doi.org/10.3390/pr11020299.
[14] V. Bächle, M. Gleiß, H. Nirschl, Influence of particles on the roller discharge of thin-film filtration without gas throughput, Chem. Eng. Technol. 47 (2024) 192–199, https://doi.org/10.1002/ceat.202300249.
[15] B. Díez, R. Rosal, A critical review of membrane modification techniques for fouling and biofouling control in pressure-driven membrane processes, Nanotechnol. Environ. Eng. 5 (2020), https://doi.org/10.1007/s41204-020-00077-x.
[16] M.W. Hakami, A. Alkhudhiri, S. Al-Batty, M.-P. Zacharof, J. Maddy, N. Hilal, Ceramic microfiltration membranes in wastewater treatment: filtration behavior, fouling and prevention, Membranes (Basel) 10 (2020), https://doi.org/10.3390/membranes10090248.
[17] S. Ripperger, Mikrofiltration mit Membranen: Grundlagen, Verfahren, Anwendungen, 1. Aufl., VCH, Weinheim, 1992. ISBN 3–527–28457-5.
[18] K. Kawashima, M. Shirzadi, T. Fukasawa, K. Fukui, T. Tsuru, T. Ishigami, Numerical modeling for particulate flow through realistic microporous structure of microfiltration membrane: direct numerical simulation coordinated with focused ion beam scanning electron microscopy, Powder Technol. 410 (2022) 117872, https://doi.org/10.1016/j.powtec.2022.117872.
[19] M.K. Borg, D.A. Lockerby, K. Ritos, J.M. Reese, Multiscale simulation of water flow through laboratory-scale nanotube membranes, J. Membr. Sci. 567 (2018) 115–126, https://doi.org/10.1016/j.memsci.2018.08.049.
[20] R. Hesse, P. Lösch, S. Antonyuk, CFD-DEM analysis of internal packing structure and pressure characteristics in compressible filter cakes using a novel elastic–plastic contact model, Adv. Powder Technol. 34 (2023) 104062, https://doi.org/10.1016/j.apt.2023.104062.
[21] B. Haddadi, C. Jordan, M. Miltner, M. Harasek, Membrane modeling using CFD: combined evaluation of mass transfer and geometrical influences in 1D and 3D, J. Membr. Sci. 563 (2018) 199–209, https://doi.org/10.1016/j.memsci.2018.05.040.
[22] S. Boldt, D. Lerche, M. Loginov, Analytical Photo-Centrifugal Filtration (ACF): Membrane Resistance and Filterability. *Filtrieren & Separieren International Edition*, 2020, pp. 15–21.
[23] M. Loginov, F. Samper, G. Gésan-Guiziou, T. Sobisch, D. Lerche, E. Vorobiev, Centrifugal ultrafiltration for determination of filter cake properties of colloids, J. Membr. Sci. 536 (2017) 59–75, https://doi.org/10.1016/j.memsci.2017.04.064.
[24] M. Loginov, N. Lebovka, E. Vorobiev, Multistage centrifugation method for determination of filtration and consolidation properties of mineral and biological suspensions using the analytical photocentrifuge, Chem. Eng. Sci. 107 (2014) 277–289, https://doi.org/10.1016/j.ces.2013.12.011.
[25] M. Loginov, A. Zierau, D. Kavianpour, D. Lerche, E. Vorobiev, G. Gésan-Guiziou, S. Mahnic-Kalamiza, T. Sobisch, Multistep centrifugal consolidation method for characterization of filterability of aggregated concentrated suspensions, Sep. Purif. Technol. 183 (2017) 304–317, https://doi.org/10.1016/j.seppur.2017.03.067.
[26] M. Loginov, F. Samper, G. Gésan-Guiziou, T. Sobisch, D. Lerche, E. Vorobiev, Characterization of membrane fouling via single centrifugal ultrafiltration, J. Taiwan Inst. Chem. Eng. 94 (2019) 18–23, https://doi.org/10.1016/j.jtice.2017.10.027.
[27] J.W. Tichy, Zum Einfluss des Filtermittels und der auftretenden Interferenzen zwischen Filterkuchen und Filtermittel bei der Kuchenfiltration, Zugl.: Kaiserlautern, Techn. Univ., Diss., Als Ms. gedr; VDI-Verl., Düsseldorf, 2007.
[28] D. Hund, P. Lösch, M. Kerner, S. Ripperger, S. Antonyuk, CFD-DEM study of bridging mechanisms at the static solid-liquid surface filtration, Powder Technol. (2020) 600–609, https://doi.org/10.1016/j.powtec.2019.11.072.
[29] D. Lerche, Comprehensive characterization of nano- and microparticles by in-situ visualization of particle movement using advanced sedimentation techniques, KONA 36 (2019) 156–186, https://doi.org/10.14356/kona.2019012.
[30] B. Radel, M. Funck, T.H. Nguyen, H. Nirschl, Determination of filtration and consolidation properties of protein crystal suspensions using analytical photocentrifuges with low volume samples, Chem. Eng. Sci. 196 (2019) 72–81, https://doi.org/10.1016/j.ces.2018.12.019.